A Benzaldehyde Derivative Obtained from *Hypoxylon truncatum* NBRC 32353 Treated with Hygromycin B

Hitoshi Kamauchi[1]*, Mitsuaki Suzuki[2], Koichi Takao[1], Yoshiaki Sugita[1]

[1]Department of Pharmaceutical Sciences, Faculty of Pharmacy and Pharmaceutical Sciences, Josai University, 1-1 Keyaki-dai, Sakado, Saitama 350-0295, Japan

[2]Department of Chemistry, Faculty of Science, Josai University, 1-1 Keyaki-dai, Sakado, Saitama 350-0295, Japan

* To whom correspondence should be addressed. E-mail: kamauchi@josai.ac.jp.

KEYWORDS

Hypoxylon truncatum/Biosynthesis/Hygromycin B/ Xylariaceae /Benzaldehyde/Monoamine oxidase

ABSTRACT

The ribosome-targeted antifungal agent hygromycin B (HygB) alters the secondary metabolite profiles of fungi. *Hypoxylon truncatum* NBRC 32353 fermented in the presence of hygromycin B in barley medium activated secondary metabolite synthesis. A new benzaldehyde derivative truncaaldehyde (**1**) was obtained, along with thirteen known compounds (**2-14**). The structures of the new compounds were revealed using NMR and single-crystal X-ray crystallography. The total synthesis of (±)-**1** was achieved using a four-step sequence, and chiral separation was accomplished. The isolated compounds were tested for their monoamine oxidase (MAO) -A and -B inhibitory activities, with six compounds ((±)-**1**, **4**, **5**, **7**, **8** and **10**) showing inhibitory activity.

Introduction

Microbes were much diversity in secondary metabolisms. They were adaptable for various survival conditions and different genes for secondary metabolisms were activated in each condition (ref. 1, 2). Gaining drug resistant was one of the adaptations to survival condition. Rifampicin resistant *Streptomyces* sp. had a mutation of RNA polymerase β-subunit genes. This mutation modulate bacterial gene expression, including natural product biosynthetic pathways and yielded new alkaloids inducamide A–C (ref. 3).

Hygromycin B (HygB) is the antifungal agents targeted to ribosome and inhibiting protein producing. Mutants resistant to ribosome-targeted drugs frequently possess mutations within a ribosomal component. This mutation could also change fungal secondary metabolisms (ref. 4).

Most microbial genes involved in secondary metabolite production are not expressed under laboratory growth conditions. These silent genes can be activated by epigenetic modulating agents such as histone deacetylase inhibitors (ref. 5). HygB also could activate fungal secondary metabolites without mutating the ribosomal DNA sequence like to epigenetic modulating agents. The production of secondary metabolites of *Fusarium* sp. RK97-94 was induced by HygB. HygB could activate self-resistance gene for a toxic secondary metabolites and compounds that were not expressed under laboratory growth conditions were discovered (ref. 6). Therefore, addition of HygB in the culture medium might induce new fungal secondary metabolites.

Fungi from the family Xylariaceae produce a variety of structurally unusual secondary metabolites (ref. 7). Benzo[*j*]fluoranthene derivatives isolated from *Hypoxylon* and *Annulohypoxylon* spp. show anti-angiogenesis activity (ref. 8, 9 and 10). The fruiting bodies of mushrooms can be harvested only during certain seasons. In Japan, fruiting bodies of *H. truncatum*

usually grow in the autumn. Fungal-type mushrooms are easy to grow in the laboratory year-round, making fungal-type mushrooms an attractive resource for chemical investigation.

In this study, we report the examination of secondary metabolites of fungal-type *H. truncatum* NBRC 32353 treated with HygB and evaluate their monoamine oxidase inhibitory activities.

Results

Fermentation of *H. truncatum* NBRC 32353

H. truncatum was fermented under several conditions, including agar (PGY agar medium; 2% peptone, 2% glucose, 1% yeast extract and 2% agar), liquid (PGY agar medium; 2% peptone, 2% glucose and 1% yeast extract), and solid media (Barley medium; 200 g of commercially available barley immersed with distilled water in a 1000 mL Roux flask). Barley medium provided the most efficient fermentation and the largest amount of extract. The phenotype of the original *H. truncatum* was white mycelia but under HygB conditions (200 g of barley immersed with distilled water containing HygB at a concentration of 31.2 μg/mL in a 1000 mL Roux flask) the color of barley was changed to yellow under the presence of HygB. HPLC profiles for a $CHCl_3$ extract of *H. truncatum* showed differences in secondary metabolites. The $CHCl_3$ extract from the barley medium without HygB showed principal constituent peaks around retention time of 32.0, 34.5 and 52.5 min, whereas the extract from *H. truncatum* fermented in the presence of HygB exhibited several newly discovered peaks (Figure 1).

Isolation

The $CHCl_3$ extract of *H. truncatum* NBRC32353 fermented under 31.2 μg/mL of HygB was subjected to silica-gel column chromatography (Si C. C.), octadecylsilyl silica-gel (ODS) C. C.,

and preparative HPLC. A pair of racemic compounds (±)-truncaaldehyde (**1**) was obtained along with thirteen known compounds. The structures of the known compounds brasilane D (**2**) (ref. 11), brasilane A (**3**) (ref. 11), trichobrasilenol (**4**) (ref. 12), 8-methoxy-1-naphthol (**5**) (ref. 13), sphaeropsidin A (**6**) (ref. 14), 5-hydroxy-8-methoxy-1-naphthol (**7**) (ref. 15), 3-methylorcilaldehyde (**8**) (ref. 16), xylarenone (**9**) (ref. 17), diketopiperazines (**10-13**) (ref. 18, 19, 20 and 21) and phenylethane-1,2-diol (**14**) (ref. 22) were identified on the basis of their spectroscopic data, as well as by comparison with published data (Figure 2).

Structure elucidation of (±)-truncaaldehyde (**1**)

(±)- Truncaaldehyde (**1**) was obtained as colorless needles by liquid-liquid diffusion using ethyl acetate and *n*-hexane. The molecular formula $C_{14}H_{20}O_5$ was determined the basis of HRFABMS. The IR spectrum of **1** suggested the presence of hydroxy group (3419 cm^{-1}) and carbonyl group (1635 cm^{-1}). The ^1H NMR spectrum showed signals attributable to four methyl protons at δ_H 2.06 (s, 3-Me), δ_H 2.56 (s, 6-Me), δ_H 1.30 (s, H-4'), and δ_H 1.35 (s, H-5'), a pair of oxy methylene protons at δ_H 4.10 (dd, J = 9.6, 7.4 Hz, H-1') and δ_H 4.22 (dd, J = 9.6, 3.2 Hz, H-1'), an aromatic proton at δ_H 6.28 (s, H-5), an aldehyde derived proton at δ_H 10.13 (s, 1-CHO), an oxymethine proton at δ_H 3.85 (dd, J = 7.4, 3.2 Hz, H-2') and a chelated hydroxyl group at δ_H 12.41 (s, 2-OH). The ^{13}C-NMR spectra showed four methyl groups at δ_C 7.3 (3-Me), δ_C 18.4 (6-Me), δ_C 25.1 (C-4') and δ_C 26.6 (C-5'), three carbons bonded to oxygen at δ_C 69.5 (C-1'), δ_C 76.7 (C-2') and δ_C 71.6 (C-3'), six aromatic carbons at δ_C 113.7 (C-1), δ_C 162.9 (each C-2 and C-4), δ_C 111.4 (C-3), δ_C 105.9 (C-5) and δ_C 141.6 (C-6) and an aldehyde at δ_C 193.3 (1-CHO) (Table. 1).

These spectral data suggested that compound **1** comprised a five-substituted benzaldehyde (C-1 to C-6) and a hydroxylated prenyl (C-1' to C-5') group. HMBC spectra showed correlations from

H-5 to C-4, 1-CHO to C-1, 2-OH to C-1 and C-2, 3-Me to C-3 and C-4, 6-Me to C-1, C-5 and C-6, H-5' to C-2', and a weak correlation from H-1' to C-4. These data indicated a planar structure of **1** comprising a 3-methylorcilaldehyde with a 2',3'-dihydroxyprenyl moiety connected to C-4 (Figure 3). We succeeded in the single-crystal X-ray crystallography of **1**, which has a chiral center at C-2'. This result showed **1** was a racemic mixture because the crystal structure of **1** has the centric space group *C*2/*c* (#15). (Figure 4, Figure S9).

Synthesis and chiral separation of (±)- truncaaldehyde (**1**)

To determine its absolute configuration, the total synthesis of (±)-**1** and its separation using chiral HPLC were performed. The novel benzaldehyde (±)-**1** was synthesized from commercially available 4-methylorcinol (**15**) using a four-step sequence (Scheme 1). Formylation was conducted using $POCl_3$/DMF to yield aldehyde (**8**). The prenyl ether at C-4 (**16**) was obtained by reaction using prenyl bromide and K_2CO_3. Epoxidation at C-2' to C-3' using *m*CPBA provided **17**. Finally, ring opening using HCl yielded (±)-**1** as colorless needles. The NMR data for synthetic (±)-**1** matched those for the isolated natural product.

The antipodes **1a** and **1b** were separated as scalemic mixture by chiral phase HPLC (Figure S10). These scalemic mixtures were optically active and their optical rotation was $[\alpha]_D^{19}$ +17.2 (MeOH *c* 0.005, **1a**) and $[\alpha]_D^{19}$ −38.4 (MeOH *c* 0.0025, **1b**) respectively. The absolute configurations of **1a** and **1b** were considered by comparing their optical rotation with the calculated rotation. The calculated optical rotation for (2'*S*)-**1** and experimental **1b** showed a negative orientation ((2'*S*)-**1** −95.9, **1b** −38.4), suggesting that the absolute configuration of **1b** was 2'*S*. In contrast, the absolute configuration of **1a** was 2'*R*.

Biological activity

Monoamine oxidases A and B (MAO-B) play a critical role in neurological disease. The MAO-A inhibitor moclobemide is a moderately effective antidepressant drug (ref. 23). The MAO-B inhibitors selegiline and resagiline are approved treatments for Parkinson's disease worldwide (ref. 24).

MAO-A and -B inhibitory tests were performed using the isolated compounds, initially at concentrations of 25 and 100 μM. The IC_{50} values of the compounds that inhibited MAO-A or -B over 50% at 25 μM were tested (Table 2). The MAO-A inhibitory test showed that five compounds (**1**, **4**, **5**, **7** and **8)** were active and their IC_{50} values were 19.0, 6.1, 1.6, 3.4 and 1.1 μM, respectively. Four compounds (**6**, **10**, **12** and **14**) showed mild inhibitory activity. The MAO-B inhibitory test showed that four compounds (**4**, **5**, **8** and **10**) were active, with IC_{50} values of 5.4, 13.7, 25.5 and 24.8 μM, respectively. Three compounds (**2**, **6** and **12**) showed mild inhibitory activity. Compound **4** equally inhibited both MAO-A and -B, whereas **1**, **7** and **8** showed MAO-A selectivity. In contrast, only **10** showed MAO-B selectivity.

Discussion

The isolated compounds were categorized as being newly synthesized by HygB activation or as being biosynthesized under the original condition. The HPLC data suggested that the peaks for all isolated compounds except **5** and **6** were observed or increased in intensity under HygB conditions. Based on the structures of the isolated compounds and the HPLC data, we speculated regarding the biosynthetic pathway activated. The biosynthetic pathway for **1** was similar to their total synthetic process. Starting compound **8** was biosynthesized from a malonyl CoA, three acetyl CoA and an *S*-adenosyl methionine. Prenylation at 4-OH, epoxidation at C-2' to C-3' and ring-opening

of the epoxide generated (±)-**1**. Based on the HPLC profiles, the production of **8** was increased, indicating that this biosynthetic pathway was newly activated by HygB.

In bioactivity for MAO-A or -B the presence of a hydroxyl group at C-5 in the naphthalene derivatives (**5** and **7**) showed different inhibitory activities: **7** showed only MAO-A inhibitory activity, but **5** inhibited both MAO-A and B activity. In the brasilane sesquiterpenoids **2**-**4**, only the aglycone **4** showed both MAO-A and B inhibitory activity. The benzaldehyde derivatives (**1** and **8**) showed inhibitory activity with MAO-A selectivity.

In conclusion, activation of secondary metabolism in *H. truncatum* by HygB resulted in the production of MAO-A and -B inhibitors and new compounds. The activation method involved the addition of HygB to normal fermentation medium is usually used for liquid medium. Our results discovered activation with HygB was also effective for solid medium. This method is promising for the discovery of new natural and medicinal lead compounds.

Materials and Methods

General and Experimental Procedures

All reagents and solvents were purchased from commercial suppliers and used without further purification. Melting points were determined on a MP apparatus (Yanaco Technical Science Corp., Tokyo, Japan). Optical rotation was measured with a P-2000 polarimeter (Jasco Corp., Tokyo, Japan). IR spectra were recorded with a FT/IR-4600typeA spectrophotometer (KBr, Jasco Corp.). UV spectra were recorded with a UV-1280 spectrophotometer (Shimazu Corp., Kyoto Japan). 1D and 2D NMR spectra were measured with a Varian 400-MR (400 MHz) spectrometer (Agilent Technologies Japan, Ltd., Tokyo, Japan), using tetramethylsilane as the internal standard. Low- and high-resolution EI and FABMS spectra were measured with a JMS-700 spectrometer (JEOL,

Tokyo, Japan). Column chromatography was performed using Wakogel C-200 (FUJIFILM Wako Pure Chemical Corporation, Osaka, Japan) and ODS silica gel (YMC-GEL ODS-A, YMC Co., Ltd., Kyoto, Japan). Analytical and preparative HPLC was performed on a Jasco PU-4580 equipped with a Jasco UV-4570 detector (Jasco Corp.) at 210 nm (analytical) and 254 nm (preparative). Preparative HPLC columns were a PEGASIL ODS sp100 column (ϕ10 × 250 mm, 5 μm, Senshu Scientific Co. Ltd., Tokyo, Japan) and a CHIRALCELL OD-H column (ϕ4.6 × 250 mm, 5 μm, Daicel Corp., Osaka, Japan). X-ray diffraction measurements were performed at 90 K on a Bruker D8 Venture diffractometer equipped with a PHOTON II detector with Mo Kα radiation (λ = 0.71073 Å, Bruker Japan K.K., Kanagawa, Japan).

Fermentation and extraction

The fungus *H. truncatum* NBRC32353 was purchased from the Biotechnology Center of the National Institute of Technology and Evaluation (Chiba, Japan). *H. truncatum* NBRC32353 was pre-incubated on PGY agar medium (2% peptone: Kyokuto Pharmaceutical Industrial, Tokyo, Japan; 2% glucose: FUJIFILM Wako Pure Chemical Corp.; 1% yeast extract: Becton Dickinson and Company, Franklin Lakes, NJ and 2% agar: Becton Dickinson and Company) at 27°C. After pre-incubation, *H. truncatum* NBRC32353 was inoculated into 1000 mL Roux flasks (12 flasks) containing barley (200 g per flask, Hakubaku, Yamanashi, Japan) immersed in hygromycin B dissolved in water (31.2 μg/mL). Flasks were statically incubated at 26°C for 28 days. The fermented substrate was extracted with $CHCl_3$.

Analytical HPLC conditions

The analytical HPLC column was a CAPCELL PAK C18 ACR column (ϕ4.6 × 250 mm, 5 μm, Osaka Soda Co., Ltd., Osaka, Japan). The solvent conditions were acetonitrile and water (0–10 min: 20:80, 10–50 min: from 20:80 to 100:0, 50–60 min: 100:0) and the flow rate was 1.0 mL/min. The $CHCl_3$ extracts obtained following growth with or without HygB were dissolved at a concentration of 1 mg/mL, and 50 μL was injected onto the column. Following purification, the isolated compounds were each dissolved at a concentration of 1 mg/mL, and 20 μL was injected for analysis.

Isolation and purification

The $CHCl_3$ extract (18.8 g) was fractionated by silica-gel column chromatography (Si C. C.) with $CHCl_3$/MeOH (100:1, 50:1, 25:1 and 10:1, followed by MeOH) to yield five fractions (a-e). Fraction a (3.4 g) was further subjected to Si C. C. (*n*-Hex/EtOAc) and octadecylsilyl (ODS) C. C. (MeOH/H_2O), yielding the six fractions aa-af. Compounds **4** (30.4 mg), **5** (279.6 mg) and **6** (10.8 mg) were isolated as fraction aa, ac and ae. Fraction b (1.8 g) was subjected to Si C. C. (*n*-Hex/EtOAc) to yield eight fractions (ba-bi). Compound **1** (40.3 mg) was obtained from fraction bd (164.0 mg) by ODS C. C. (MeOH/H_2O). ODS C. C. (MeOH/H_2O) and preparative HPLC of fraction bb (300.5 mg) yielded **7** (4.2 mg, t_R 15 min) and **8** (2.7 mg, t_R 18 min). ODS C. C. (MeOH/H_2O) of fraction bf (213.1 mg) yielded six fractions, and **9** (25.4 mg) was isolated as fraction bfb. Preparative HPLC for fraction bfe (95.7 mg) yielded **10** (19.1 mg, t_R 14 min), **11** (2.0 mg, t_R 18 min) and **12** (33.4 mg, t_R 20 min). Fraction bi (374.7 mg) subjected to Si C. C. ($CHCl_3$/MeOH) to yield **13** (139.2 mg). Fraction c (1.2 g) was subjected to Si C. C. ($CHCl_3$/MeOH) and ODS C. C. (MeOH/H_2O) to yield **14** (42.0 mg). Fraction d (477.7 mg) Si C. C. ($CHCl_3$/MeOH) and ODS C. C. (MeOH/H_2O) yielded **2** (8.7 mg) and **3** (52.4 mg).

Compound **1** (3.0 mg) was subjected to chiral phase HPLC with *n*-Hex/isopropanol (15:1), yielding **1a** (0.6 mg, t_R 16 min) and **1b** (0.3 mg, t_R 17.5 min) as scalemic mixture.

(±)- Truncaaldehyde (**1**)

Colorless needles, m.p. 90-92°C, $[\alpha]_D^{19}$ +17.2 (MeOH *c* 0.005, **1a** (2'*R*)), $[\alpha]_D^{19}$ −38.4 (MeOH *c* 0.0025, **1b** (2'*S*)), UV (MeOH) λ_{max} (log ε) 206 (4.01), 296 (4.05) nm, IR (KBr) υ_{max} 3419, 2964, 1635 cm^{-1}, ^1H and ^{13}C NMR data, see Table 1. HRFABMS *m/z* 269.1390 $[M+H]^+$ (calculated for $C_{14}H_{21}O_5$, 269.1389).

Synthesis of (±)-**1**.

Preparation of **16**

Compound **8** was prepared using the same procedure performed by Summer *et al.* (ref. 16). To a solution of **8** (210.0 mg, 1.27 mmol) in acetone (10.0 mL) was added potassium carbonate (282.4 mg 2.05 mmol) and 3,3-dimethylallyl bromide (290.3 mg, 1.95 mmol). The reaction mixture was stirred at room temperature for 12 h. Excess water was added and the reaction mixture was extracted using EtOAc. The organic layer was dried over Na_2SO_4, yielding **16** (164.2 mg, 0.70 mmol, 55%) after purification by Si C. C. (*n*-Hex-EtOAc 5:1).

^1H-NMR (400 MHz, $CDCl_3$) δ 12.41 (s, 2-OH), 10.11 (s, 1-CHO), 6.27 (s, H-5), 5.47 (m, H-2'), 4.59 (brd, *J* = 6.6 Hz, H-2'), 2.56 (s, 6-Me), 2.05 (s, 3-Me), 1.80 (s, H-5'), 1.75 (s, H-4'); ^{13}C-NMR (100 MHz, $CDCl_3$) δ 193.1 (1-CHO), 163.6 (C-4), 162.9 (C-2), 141.3 (C-6), 138.3 (C-3'), 119.2 (C-2'), 113.3 (C-1), 111.5 (C-3), 106.2 (C-5), 65.3 (C-1'), 25.8 (C-4'), 18.5 (C-5'), 18.3 (6-Me), 7.1 (3-Me); HRFABMS *m/z* 234.1255 $[M]^+$ (calculated for $C_{14}H_{18}O_3$, 234.1256).

Epoxidation of **16**

To a solution of **16** (100.0 mg, 0.43 mmol) in dichloromethane (5.0 mL) was added sodium hydrogen carbonate (15.0 mg, 0.18 mmol) and *m*-chloroperoxybenzoic acid (103.2 mg, 0.60 mmol). The reaction mixture was stirred at room temperature for 12 h and extracted with dichloromethane-water. The organic layer was dried over Na_2SO_4, yielding **17** (40.4 mg, 0.16 mmol, 38%) with slight impurities after purification by Si C. C. (*n*-Hex-EtOAc 5:1).

^{1}H-NMR (400 MHz, $CDCl_3$) δ 12.41 (s, 2-OH), 10.13 (s, 1-CHO), 6.28 (s, H-5), 4.23 (dd, J = 11.1, 4.4 Hz, H-1'), 4.13 (dd, J = 11.1, 5.8 Hz, H-1'), 3.16 (dd, J = 5.8, 4.4 Hz, H-2'), 2.56 (s, 6-Me), 2.08 (s, 3-Me), 1.41 (s, H-5'), 1.38 (s, H-4'); ^{13}C-NMR (100 MHz, $CDCl_3$) δ 193.3 (1-CHO), 163.0 (C-4), 159.4 (C-2), 141.5 (C-6), 120.0 (C-3), 113.6 (C-1), 106.0 (C-5), 67.5 (C-1'), 61.1 (C-2'), 58.2 (C-3'), 24.6 (C-4'), 19.1 (C-5'), 18.5 (6-Me), 7.2 (3-Me); HRFABMS *m/z* 250.1197 $[M]^+$ (calculated for $C_{14}H_{18}O_4$, 250.1205).

Epoxide ring-opening reaction of **17**

To a solution of **17** (14.0 mg 0.056 mmol) in methanol (0.5 mL) and water (0.5 mL) was added 10% HCl (0.5 mL). The reaction was stirred at room temperature for 15 min. The crude mixture was purified by Si C. C. (*n*-Hex-EtOAc 5:1) to yield (±)-**1** (6.1 mg 0.023 mmol, 41%)

X-ray crystallographic data for **1**.

Crystal data: $C_{14}H_{20}O_5$, space group $C2/c$ (#15), a = 17.3939(11) Å, b = 17.5658(11) Å, c = 10.4425(7) Å, β = 122.941(2) °, V = 2677.6(3) Å^3, Z = 8, crystal size 0.143 × 0.190 × 0.232 mm, T = 90 K, reflections collected 21249, independent reflections 3169; 2534 with $I > 2\sigma(I)$; R_1 = 0.0556 [$I > 2\sigma(I)$], wR_2 = 0.1484 (all data), GOF = 1.079. Crystallographic data for **1** reported in

this paper have been deposited at the Cambridge Crystallographic Data Centre under reference number CCDC 2093272. These data can be obtained free of charge from The Cambridge Crystallographic Data Centre via https://www.ccdc.cam.ac.uk/structures/

Computational analyses

Conformational analyses of **1b** were carried out in the MMFF94S (ref. 25 and 26) molecular mechanics force field using CONFLEX software (ref. 27, 28 and 29). The geometries obtained within a 1.0 kcal/mol energy range were further optimized using the semi-empirical PM6 (ref. 30) method available in the Gaussian 09 program (ref. 31). The geometries were further optimized by the density functional theory method at the B3LYP/6-31G (d) level (ref. 32, 33, 34 and 35) using the Gaussian 09 program package to give two predominant conformers. Optical rotation was obtained from the most stable conformation with the B3LYP/DGDZVP basis set (ref. 36).

Bioassay

MAO-A and -B inhibitory assay

MAO-A and MAO-B inhibitory activities were assayed using the method in our previous report with slight modification (ref. 37). 3 μL of human recombinant MAO-A solution (M7316, Sigma-Aldrich) or 7 μL of MAO-B solution (M7441, Sigma-Aldrich) was diluted with 1100 μL of potassium phosphate buffer (0.1 M, pH 7.4). 140 μL of potassium phosphate buffer, 8 μL of kynuramine (final concentration is 30 μM, Sigma-Aldrich, St. Louis, MO) in potassium phosphate buffer, and 2 μL of a dimethyl sulfoxide (DMSO) inhibitor solution (final DMSO concentration of 1% (v/v)), were mixed and pre-incubated at 37°C for 10 min. 50 μL of diluted MAO-A or MAO-B solution was then added to each well. The reaction mixture was further incubated at 37°C and

the reaction was stopped after 20 min by the addition of 75 μL of 2 M NaOH. The product generated by MAO-A or MAO-B, 4-quinolinol, is fluorescent and was measured at Ex 310 nm/Em 400 nm using a microplate reader (SPECTRA MAX M2, Molecular Devices, Tokyo, Japan). DMSO without test compound was used as the negative control, and pargyline (Sigma-Aldrich) was used as a positive control. The IC_{50} values were estimated using Prism software (version 5.02; GraphPad, San Diego, CA).

Supplementary information

Supplementary information (^{1}H NMR, ^{13}C NMR, 2D NMR data, for the new compounds) is available at Journal of Antibiotics website https://

Compliance with ethical standards

Conflict of interest

The authors declare that they have no conflict of interest.

Publisher's note

Springer Nature remains neutral with regard to jurisdictional claims in published maps and institutional affiliations.

References

1. Frank M, et al. Brominated azaphilones from the sponge-associated fungus *Penicillium canescens* strain 4.14.6a. *J. Nat. Prod.* 2019;82:2159-2166.

2. Kamauchi H, Kinoshita K, Sugita T, Koyama K. Conditional changes enhanced production of bioactive metabolites of marine derived fungus *Eurotium rubrum*. *Bioorg. Med. Chem. Lett.* 2016;26:4911-4914.

3. Fu P, Jamison M, La S, MacMillan JB. Inducamides A-C, chlorinated alkaloids from an RNA polymerase mutant strain of *Streptomyces* sp. *Org Lett.* 2014;16:5656-5659.

4. Ochi K, et al. Ribosome engineering and secondary metabolite production. *Adv Appl Microbiol.* 2004;56:155-184.

5. Asai T, Morita S, Taniguchi T, Monde K, Oshima Y. Epigenetic stimulation of polyketide production in *Chaetomium cancroideum* by an NAD(+)-dependent HDAC inhibitor. *Org Biomol. Chem.* 2016;14:646-651.

6. Kato S, et al. Induction of secondary metabolite production by hygromycin B and identification of the 1233A biosynthetic gene cluster with a self-resistance gene. *J. antibiot.* 2020;73:475–479.

7. Helaly SE, Thongbai B, Stadler M. Diversity of biologically active secondary metabolites from endophytic and saprotrophic fungi of the ascomycete order Xylariales. *Nat. Prod. Rep.* 2018;35:992-1014.

8. Koyama K, Kuramochi D, Kinoshita K, Takahashi K. Hypoxylonols A and B, novel reduced benzo[*j*]fluoranthene derivatives from the mushroom *Hypoxylon truncatum*. *J. Nat. Prod.* 2002;65:1489-1490.

9. Fukai M, et al. Hypoxylonols C-F, benzo[*j*]fluoranthenes from *Hypoxylon truncatum*. *J. Nat. Prod.* 2012 ;75:22-25.

10. Fukai M, et al. Antiangiogenic activity of hypoxylonol C. *J. Nat. Prod.* 2014;77:1065-1068.

11. Feng J, et al, Biosynthesis of oxygenated brasilane terpene glycosides involves a promiscuous *N*-acetylglucosamine transferase. *Chem Commun*. 2020;56:12419-12422.

12. Murai K, et al. An unusual skeletal rearrangement in the biosynthesis of the sesquiterpene trichobrasilenol from *Trichoderma*. *Angew Chem Int Ed Engl.* 2019;58:15046-15050.

13. Banerjee A, et al. Transformation of 5-methoxy-1-tetralone into 8-methoxy-1-tetralone. *J. Chem. Res.* 2010;34:522-524.

14. Antonio E, et al. A phytotoxic pimarane diterpene of *Sphaeropsis sapinea* f. sp. *Cupressi*, the pathogen of a canker disease of cypress. *Phytochem.* 1996;42:1541-1546.

15. Hartmut L., Synthese dimerer juglone und methyljuglone, *Tetrahedron Lett.* 1976;17:3287-3290. The NMR data was not shown in the reference. The structure was revealed by using 1D and 2D NMR data. These data were available in the supporting data.

16. Baker Dockrey SA, Lukowski AL, Becker MR, Narayan ARH. Biocatalytic site- and enantioselective oxidative dearomatization of phenols. *Nat. Chem.* 2018;10:119-125.

17. Rukachaisirikul V, et al. Metabolites from the xylariaceous fungus PSU-A80. *Chem. Pharm. Bull.* 2007;55:1316-1318.

18. Xi YK, et al. Total synthesis of spirotryprostatins through organomediated intramolecular umpolung cyclization. *Chemistry.* 2019;25:3005-3009.

19. Maciel OMC, Tavares RSN, Caluz DRE, Gaspar LR, Debonsi HM. Photoprotective potential of metabolites isolated from algae-associated fungi *Annulohypoxylon stygium*. *J. Photochem. Photobiol. B.* 2018;178:316-322.

20. Arunrattiyakorn P, Ikeda B, Nitoda T, Kanzaki H. Enzymatic synthesis of dehydroderivatives from proline-containing cyclic dipeptides and their effects toward cell division. *Biosci. Biotechnol. Biochem.* 2007;71:830-833.

21. Daniela H, Sabine L, Angelika B, Wolfgang F. Diastereoselective alkylation of a proline-derived bicyclic lactim ether. *Helvetica Chimica Acta.* 2006;89:1894-1909

22. Plietker B, Niggemann M, Pollrich A. The acid accelerated ruthenium-catalysed dihydroxylation. Scope and limitations. *Org. Biomol. Chem.* 2004;2:1116-1124.

23. Chiuccariello L, et al. Monoamine oxidase-A occupancy by moclobemide and phenelzine: implications for the development of monoamine oxidase inhibitors. *Int. J. Neuropsychopharmacol.* 2015;19:pyv078.

24. Cereda E, et al. Efficacy of rasagiline and selegiline in parkinson's disease: a head-to-head 3-year retrospective case-control study. *J. Neurol.* 2017;264:1254-1263.

25. Halgren TA. Merck molecular force field. I. basis, form, scope, parameterization, and performance of MMFF94. *J. Comput. Chem.* 1996;17:490–519.

26. Halgren TA. MMFF VII. Characterization of MMFF94, MMFF94s, and other widely available force fields for conformational energies and for intermolecular-interaction energies and geometries. *J. Comput. Chem.* 1999;20:720–729.

27. Goto H, Osawa E. Corner flapping: a simple and fast algorithm for exhaustive generation of ring conformations. *J. Am. Chem. Soc.* 1989;111:8950–8951.

28. Goto H, Osawa E. An efficient algorithm for searching low-energy conformers of cyclic and acyclic molecules. *J. Chem. Soc., Perkin Trans. 2.* 1993;187–198.

29. Goto H, et al, *Conflex Corp.,* Tokyo, JAPAN 2004.

30. Stewart JJP, Optimization of parameters for semiempirical methods V: Modification of NDDO approximations and application to 70 elements. *J. Mol. Model.* 2007;13:1173–1213.

31. Frisch MJ, et al. Gaussian 09; Gaussian, Inc.: Wallingford, CT, USA, 2013

32. Becke AD, Density‐functional thermochemistry. III. The role of exact exchange. *J. Chem. Phys.* 1993;98:5648–5652.

33. Lee C, Yang W, Parr RG, Development of the Colle-Salvetti correlation-energy formula into a functional of the electron density. *Phys. Rev. B.* 1988;37:785–789.

34. Miehlich B, Savin A, Stoll H, Preuss H, Results obtained with the correlation energy density functionals of becke and Lee, Yang and Parr. *Chem. Phys. Lett.* 1989;157:200–206.

35. Stephens PJ, Devlin FJ, Chabalowski CF, Frisch MJ, Ab Initio calculation of vibrational absorption and circular dichroism spectra using density functional force fields. *J. Phys. Chem.* 1994;98:11623–11627.

36. Godbout N, Salahub D, Andzelm J, Wimmer E, Optimization of Gaussian-type basis sets for local spin density functional calculations. Part I. Boron through neon, optimization technique and validation. *Can. J. Chem.* 1992;70:560–571.

37. Kamauchi H, Oda T, Horiuchi K, Takao K, Sugita Y. Synthesis of natural product-like polyprenylated phenols and quinones: Evaluation of their neuroprotective activities. *Bioorg Med Chem.* 2020;28:115156.

Figure legends

Fig. 1 HPLC profiles of the $CHCl_3$ ext. of *H. truncatum* cultured on barley medium with and without HygB.

Fig. 2 Chemical structures of compounds **1–14**.

Fig. 3 HMBC correlations of **1**.

Fig. 4 X-ray crystal structure of **1**.

Scheme legends

Scheme 1 Synthesis of (±)-**1**

Table legends

Table 1 NMR spectroscopic data of **1**.

Table 2 Inhibitory effects of compounds **1**−**14** on MAO-A and -B.

Fig. 1

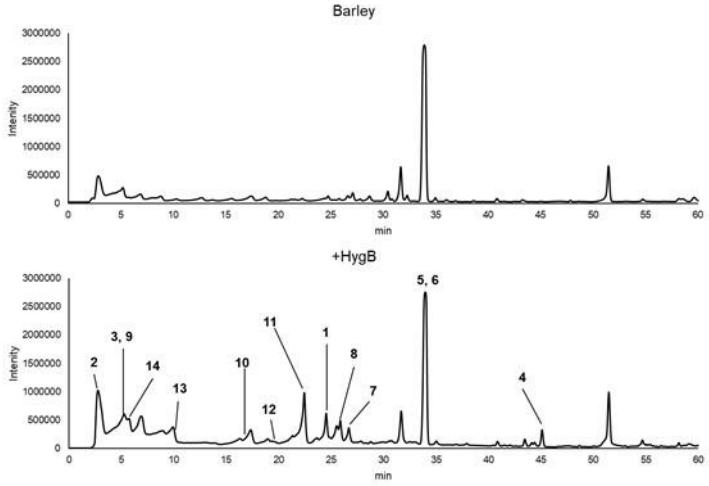
Barley
Intensity
min
+HygB
2
3, 9
14
13
10
12
11
1
8
7
5, 6
4

Fig. 2

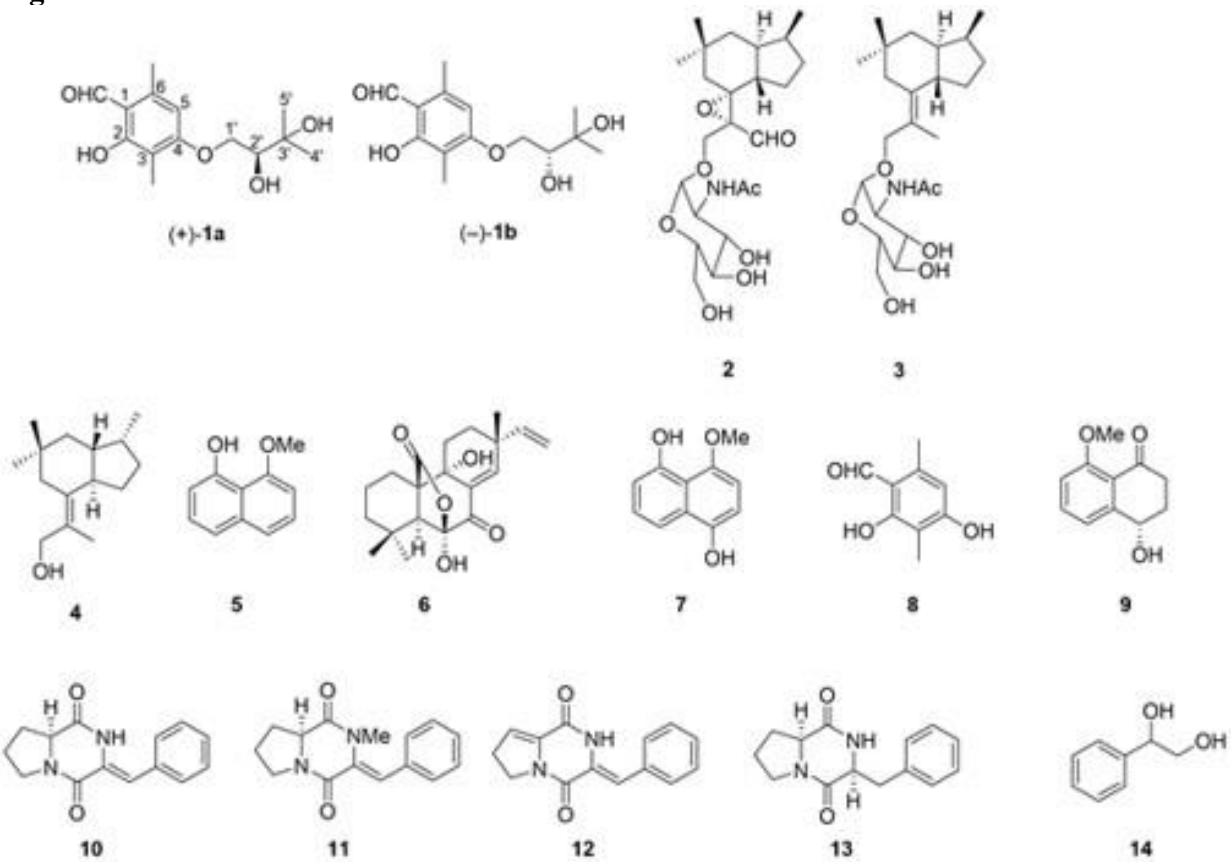
(+)-1a
(–)-1b
2
3
4
5
6
7
8
9
10
11
12
13
14

Fig. 3

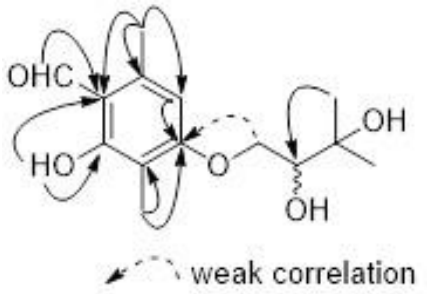

1

Fig. 4

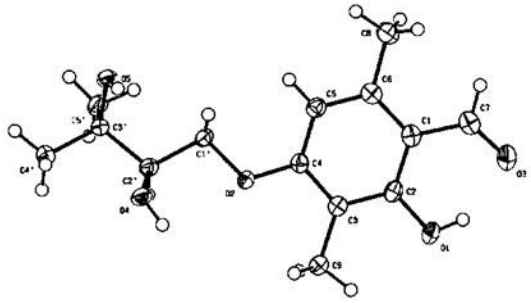

Scheme 1

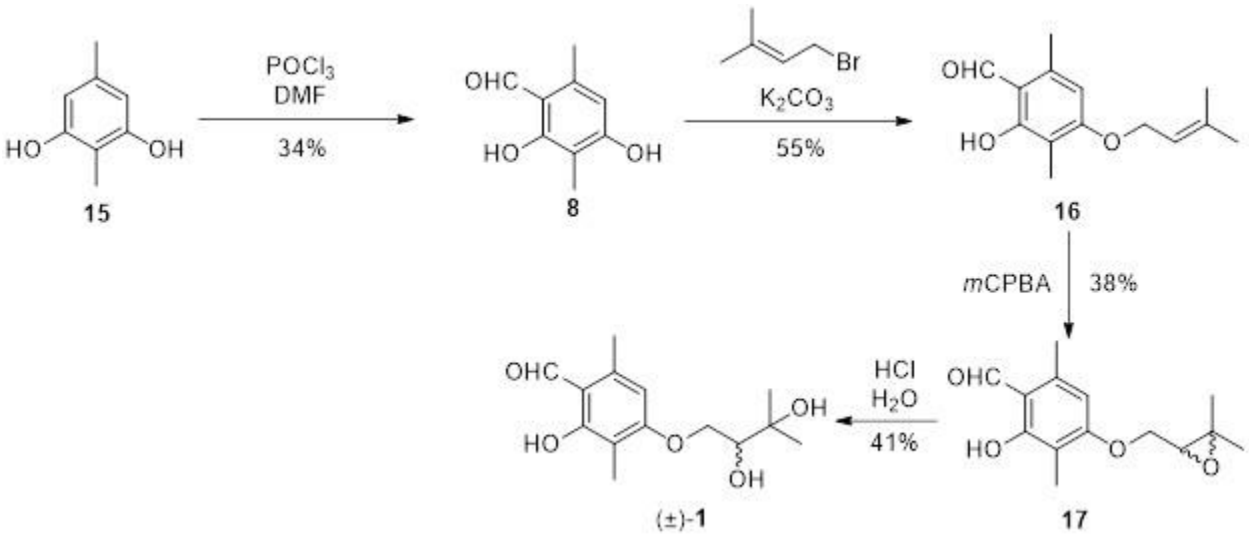

Table 1

truncaaldehyde (**1**)		
Pos.	δ_C	δ_H (*J* in Hz)
1	113.7	
2	162.9[a]	
3	111.4	
4	162.9[a]	
5	105.9	6.28 (s)
6	141.6	
1-CHO	193.3	10.13 (s)
3-Me	7.3	2.06 (s)
6-Me	18.4	2.56 (s)
1'	69.5	4.10 (dd, 9.6, 7.4)
		4.22 (dd, 9.6, 3.2)
2'	76.7	3.85 (dd, 7.4, 3.2)
3'	71.6	
4'	25.1	1.30 (s)
5'	26.6	1.35 (s)
2-OH		12.41 (brs)
2'-OH		2.30 (brs)[b]
3'-OH		2.75 (brs)[b]

Measured in $CDCl_3$, [a, b] may be interchanged between two signals.

Table 2

	MAO-A			MAO-B			
	Inhibition rate (%, Mean ± SE)		IC_{50} (μM)	Inhibition rate (%, Mean ± SE)		IC_{50} (μM)	selectivity[c]
	25 μM	100 μM		25 μM	100 μM		
1	52.9±0.6	86.0±0.4	19.0	n.d.	44.7±0.7	n.d.	MAO-A
2	n.d.	28.6±2.5	n.d.	28.7±1.3	53.8±0.6	n.d.	
3	n.d.	n.d.[b]	n.d.	n.d.	20.2±1.9	n.d.	
4	79.9±0.8	96.1±0.2	6.1	84.1±0.5	94.4±0.0	5.4	
5	93.2±0.5	98.2±0.6	1.6	70.9±1.4	94.3±0.7	13.7	
6	33.7±0.6	78.6±1.2	n.d.	30.1±3.0	69.5±0.7	n.d.	
7	87.9±1.4	97.0±0.1	3.4	n.d.	30.4±2.5	n.d.	MAO-A
8	96.7±0.6	99.1±0.9	1.1	50.9±1.3	88.0±0.3	25.5	MAO-A
9	n.d.	24.0±3.9	n.d.	n.d.	20.2±1.0	n.d.	
10	14.3±3.0	58.0±0.4	n.d.	52.9±0.7	87.2±0.2	24.8	MAO-B
11	n.d.	42.9±1.9	n.d.	n.d.	47.6±1.3	n.d.	
12	1.5±4.6	63.6±0.6	n.d.	9.4±4.5	88.0±0.0	n.d.	
13	n.d.	10.2±1.0	n.d.	n.d.	13.0±1.7	n.d.	
14	5.7±13.9	99.6±0.5	n.d.	n.d.	8.6±2.3	n.d.	
Pargyline[a]	62.4±1.2 (10 μM)			86.9±0.3 (1 μM)			

[a] used as positive control. [b] Not determined due to the inhibition rate was under 0%. [c] IC_{50} (MAO-A)/IC_{50} (MAO-B) <0.1 (MAO-A selective), >10 (MAO-B selective).